Sensors & Actuators: A. Physical 396 (2025) 117204

Contents lists available at ScienceDirect

Sensors and Actuators: A. Physical

journal homepage: www.journals.elsevier.com/sensors-and-actuators-a-physical

Magnetic sensing modules for in-vivo blood pressure monitoring in anastomosed arteries

Menduh Furkan Aslan [a,b], Tuğba Selcen Navruz [c], Mustafa İlker Beyaz [d,*]

[a] Department of Electrical and Electronics Engineering, Gazi University, Graduate School of Natural and Applied Sciences, Ankara 06500, Turkiye
[b] Department of Electrical and Electronics Engineering, Antalya Bilim University, Antalya 07190, Turkiye
[c] Department of Electrical and Electronics Engineering, Gazi University, Ankara 06570, Turkiye
[d] Institute of Microstructure Technology, Karlsruhe Institute of Technology, Eggenstein-Leopoldshafen 76344, Germany

ARTICLE INFO

Keywords:
Blood pressure monitoring
Implantable pressure sensor
Arterial anastomosis
Hall sensor
MEMS

ABSTRACT

This paper presents the development of magnetic sensing modules designed to conformally encircle arteries for in-vivo blood pressure monitoring. The modules incorporate multiple off-the-shelf Hall sensors and permanent magnets arranged on a flexible substrate to transform arterial distention due to blood pressure into voltage. The novelty of the design lies in the multitude of components and their circular collocations that yields significant improvement in pressure sensitivity as revealed by finite element simulations. The sensors and magnets were encapsulated in biocompatible materials and assembled on a flexible PDMS substrate with metal interconnects, which are fabricated through microfabrication techniques. Test results on a latex pipe serving as the artery model demonstrated sensitivity values reaching 0.42 mV/mmHg, representing a 3.8-fold improvement over traditional single sensor-magnet pair design. Long-term tests both in air and in PBS solution showed no degradation in the sensitivity, and a high linearity with R^2 exceeding 0.98. The average sensitivity is projected to reach 3.2 mV/mmHg in-vivo due to the higher compliance of the arterial tissue. The reported results underscore the viability of this implantable device for continuous blood pressure monitoring in large arteries. This is particularly crucial in organ transplantation, where the main artery supplying blood to the transplanted organ is anastomosed and requires continuous monitoring to ensure adequate blood flow after the surgical operation.

1. Introduction

Organ transplantation is arguably one of the most vital and technologically advanced medical procedures that prevents patient mortality due to organ failure. According to reports from the World Health Organization's (WHO) Global Observatory on Donation and Transplantation platform, this procedure was performed over 170,000 times globally in 2023 [1], with numbers expected to rise in line with global population growth. A major step in organ transplantation procedure is anastomosis, where arteries are physically connected and stitched together to facilitate blood circulation through the newly transplanted organ. The blood pressure in these connected arteries serves as the primary indicator of adequate organ perfusion in the post-surgical period [2]. Accordingly, it should be continuously monitored to ensure proper organ function and allow timely surgical intervention if needed.

One commonly used blood flow and pressure monitoring techniques involves using an ultrasonic Doppler probe located on an artery that can transmit and receive sound waves to determine the speed and direction of blood flow [3]. Other solutions employing pressure transducers incorporated into catheter tips and directly inserted into the artery for monitoring pressure during surgical operations also exist [4]. Although all these approaches are useful, they are only suitable for intermittent readings as the measurement is only possible when the all the equipment is applied on patient's body, which also restrict patient movement.

A number of sensors have been developed for in-vivo pressure monitoring, where the sensor is implanted inside the body and can perform on-demand measurements. Depending on their implantation site, these sensors can be classified into two categories as intra-arterial and peri-arterial. The intra-arterial pressure sensors are located inside the artery in immediate contact with the blood, and therefore make direct pressure measurements. A prominent example in this category, which has also been commercialized, is EndoSure pressure sensor by CardioMEMS Inc [5]. The sensor is composed of inductive and

* Corresponding author.
E-mail address: mustafa.beyaz@kit.edu (M.İ. Beyaz).

https://doi.org/10.1016/j.sna.2025.117204
Received 11 July 2025; Received in revised form 9 October 2025; Accepted 23 October 2025
Available online 24 October 2025

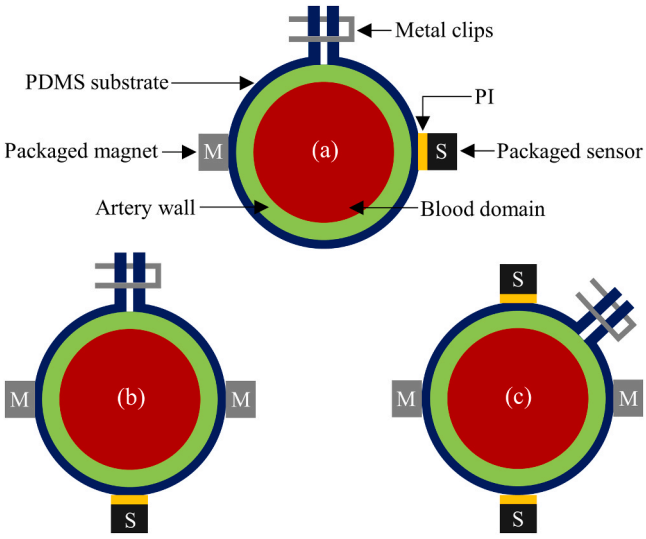

Fig. 1. Schematic of the sensor module designs, (a) D0 - basic design with a single magnet and sensor, (b) D1 - with one sensor and two magnets, (c) D2 - two magnets and two sensors.

capacitive components, and is permanently implanted into the artery using a catheter. An external antenna can communicate with the sensor to track resonant conditions and acquire pressure data. Other architectures incorporating a capacitive sensor in a metal stent also has been demonstrated, where the sensor together with the stent form a resonant LC circuit [6–8]. The pressure can then be monitored by tracking the resonant frequency shifts. Although intra-arterial sensors offer more accurate readings by enabling direct measurements, the immediate placement inside blood stream also introduces risks such as thrombosis, infection, bleeding, and vascular injury [9]. Peri-arterial sensors, on the other hand, are positioned around the artery, typically configured in a cuff-like structure. They are usually designed to detect the displacements on the arterial wall due to blood pressure variations, and hence make indirect pressure measurements. Using this design framework, various sensors with different transduction mechanisms have been presented. A resonant capacitive arterial pulse sensor design consisting of an inductor and a flexible sheet with microstructured pyramids was reported in [10]. When wrapped around an artery, the blood pressure pulsations expand and contract the pyramid structures, yielding a 0.4 % capacitance change. Another research group used accelerometers on an artery to detect the reflected blood pulse wave transit time, and showed that it correlates with blood pressure [11]. Using similar design strategies, novel devices with various transduction mechanisms including capacitive [12–15], piezoelectric [16–19], piezoresistive [20–22], optical [23,24] and impedimetric [25] have also been demonstrated.

Magnetic sensing, although not exploited as much so far, poses significant advantages compared to other transduction mechanisms mentioned above for the development of peri-arterial blood pressure sensors [26]: (i) body fluids, tissues, and biocompatible packaging have very weak and uniform magnetic properties, (ii) magnetic components are unaffected by the pressure impinging upon them, and (iii) sensing arrangement can be implemented using already available off-the-shelf components. These important advantages render measurements highly insensitive to factors other than blood pressure, arguably positioning magnetic sensing as a superior approach compared to alternative methods. To this end, a commercial Hall effect sensor and a magnet positioned right across each other was previously shown to measure arterial distension in [27]. The sensor and the magnet were immobilized on the artery with silicon strips. Correlating sensor voltage with arterial dilation due to blood pressure, a sensitivity of 0.65 mV/mmHg was reported for in-vitro experiments. Our earlier study reported in [28] aimed to achieve a higher sensitivity through the investigation of multiple magnetic components and their relative collocations. In this work, we expand upon our previous studies and present a comprehensive theoretical and experimental analysis on the sensitivity and performance of different component configurations. Several designs with varying number of Hall sensors and magnets, and their circular arrangements have been investigated through finite element simulations to enhance the magnetic flux density reduction per arterial diameter expansion. The designs have been implemented and thoroughly tested for pressure sensitivity and examined for linearity in their response. Long-term durability tests were performed for the best-performing design. The experiments clearly showed that the proposed magnetic sensor module can be implanted around an artery after anastomosis for continuous blood pressure monitoring with superior sensitivity.

2. Design and analysis

The device consists of Hall sensors and permanent magnets mounted on a flexible substrate that can comply with circular artery circumference (Fig. 1). Biocompatible materials were used for the substrate as well as for packaging individual elements. In order to avoid confusion for the reader, the complete assembly of these components together with the substrate will be referred to as “sensor module” to differentiate from a single Hall sensor, which is part of the module. The sensor module is intended to be implanted along the artery, at a location between the anastomosed site and the newly transplanted organ. During operation, blood pressure pulsations alter the artery diameter, which shifts the relative positions of magnets and the sensor. This results in oscillations on the sensor voltage that can be mapped into blood pressure pulsations through fluidic, mechanical, and magnetic properties of the blood, artery wall, and sensor, respectively. Following an initial calibration of the sensor module at the time of implantation, using a surgical-grade blood pressure sensor to align systolic and diastolic pressures as well as desired number of intermediary data points with the corresponding sensor voltages, continuous blood pressure monitoring can be performed.

Considering that the target artery diameter is on the order of 5 mm and the maximum relative artery expansion can reach only 15 % for a normal blood pressure variation [29], a compact yet highly sensitive Hall sensor should be selected to yield a large voltage variation in response to pressure oscillations. In this respect, a commercial unipolar ratiometric linear Hall effect sensor (DRV5056A1QDBZT, Texas Instruments) was chosen that has a sensitivity of 200 mV/mT, operates at voltages down to 3.3 V, and measures 1.3 × 2.92 × 1.12 mm in width, length, and thickness, respectively. The sensor also has a bandwidth of 20 kHz, well above the frequency of the pulsatile blood flow on the order

of a few Hz. The sensor is mounted on biocompatible polyimide (PI) to provide mechanical support as well as to serve as a suitable board that allows the electrical connections to the sensor pins. NdFeB-N52 grade magnets were preferred as the magnetic field source to establish a high magnetic flux density. The size of the magnets was selected to closely match that of the sensor to yield a relatively uniform mass distribution and mechanical balance. Both the sensor on PI and the magnets were mounted on a polydimethylsiloxane (PDMS) substrate that provides the required flexibility and conformity to wrap the complete sensor module around the artery. A schematic of the sensor module located on an artery is shown in Fig. 1a, where two ends of the PDMS substrate were fixed with metal clips. Although not clearly shown for the sake of image clarity, the sensor and magnet components are packaged using biocompatible epoxy, which mitigates immune system responses and inhibit the infiltration of bodily fluids into the components. This epoxy also provides a conformal coating, smoothing sharp geometric features and thereby minimizing the risk of mechanical damage to the surrounding tissue.

Various designs and configurations have been investigated to achieve a high voltage variation per unit arterial expansion. Fig. 1a shows the basic design (D0) consisting of a single sensor and a single magnet directly positioned across each other. This design was previously reported by Ruhammer et al. in [27] with a sensitivity of 0.65 mV/mmHg on a PI substrate. In our current work, different sensor-magnet configurations involving more components are investigated to improve the sensitivity. Fig. 1b shows a more advanced design (D1) that contains one sensor with two magnets arranged in a T configuration, where the same poles of the magnets face radially inwards. This configuration curves the magnetic field lines and guides them through the sensor, which also facilitates a larger field variation when the artery expands as discussed in the next section. This design was further developed to include two sensors as shown in Fig. 1c, leading to the same voltage generated on the newly-added sensor due to geometrical symmetry (D2). Summing the voltage of both sensors can theoretically double the sensitivity of the sensor module. Other combinations involving (i) different component collocations around the periphery and (ii) opposite magnetic poles facing each other were not investigated as all such configurations lead to lower fields on the sensors or magnets snapping against each other. We would like to note that further increasing the number of components in the sensor module was originally intended; however, was found to be not feasible due to space constraints and repulsive magnetic forces preventing the implementation of the module. Finally, metal clips were used to fix the sensor module on the artery (Fig. 1).

Simulations were carried out to compare the sensitivity of each design shown in Fig. 1. Initially, arterial expansion in response to pressure variations was modeled using the Fluid-Structure Interaction (FSI) module of the COMSOL finite element simulation software. In this model, the fluid exerts radially outward pressure on the inner arterial wall over a physiologically relevant range, resulting in an increase in arterial diameter. The expanded diameters corresponding to different pressure values, obtained from the FSI simulations, are then used to define the arterial geometries for the magnetic simulations, which are performed using the Magnetic Fields, No Currents interface of the AC/DC module. Due to the lack of access to a real artery and blood in our test setup, these were replaced with a latex pipe and water in the simulations to allow for a direct comparison with the test results later on. This approach is also commonly adopted in the literature [14,16,17], as the mechanical and fluidic properties of these materials are comparable. The parameters used in FSI simulations were chosen based on the corresponding material properties previously reported in [30]- [31] and listed in Table 1. Water was modeled using incompressible, laminar and Newtonian properties, while no-slip boundary condition was applied between the water and latex domains. The outer diameter of the latex pipe was set to 4.77 mm to ensure consistency with the actual component used in subsequent experiments. A linear elastic behavior with constant Young's modulus was assumed for the latex, due to small expected deformations. Since it would be computationally demanding to simulate the entire artery structure, only a 30 mm part of it was considered. The simulation model is shown in Fig. 2a. The sensors and magnets are excluded from this analysis as they do not affect the radial expansion.

Table 1
FSI Simulation parameters.

Parameter	Value	Parameter	Value
Latex Young's modulus	1200 kPa	PDMS Young's modulus	750 kPa
Latex Poisson's ratio	0.44	PDMS Poisson's ratio	0.49
Latex density	960 kg/m^3	PDMS density	970 kg/m^3
Latex length	30 mm	PDMS diameter × length	5.37 mm × 10 mm
Latex outer diameter	4.77 mm	PDMS thickness	0.3 mm
Latex wall thickness	1 mm	Water density	997 kg/m^3
Simulation duration	1 sec	Water viscosity	0.001 Pa.s
Artery Model: Mooney - Rivlin			
Arterial tissue density	1120 kg/m^3	Blood viscosity	0.0035 Pa.s
Wall thickness	0.125 – 0.8 mm	Blood density	1060 kg/m^3

The fluid pressure at every point inside the artery was ramped up to 200 mmHg to fully cover and further exceed the typical physiological range of 80–120 mmHg observed in the human body. The rise time from 0 mmHg to 200 mmHg was set to 1 s, and the pressure profile was defined using a continuous second-derivative smoothing. Shorter rise times with a linear pressure increase caused convergence issues, whereas longer rise times or more complex pressure profiles had no significant effect on the results. The displacement of the PDMS, and hence the sensors and the magnets, with respect to time is illustrated in Fig. 2b. Fig. 2c-e show the displacements of the latex and PDMS at 0, 100, and 200 mmHg, respectively. At the maximum pressure of 200 mmHg, the latex expands by 0.17 mm (from 4.77 mm to 4.94 mm), while the PDMS expands by 0.14 mm (from 5.37 mm to 5.51 mm). As expected, the PDMS region expands less than the rest of the latex due to the larger total thickness and the corresponding reduction in the overall compliance.

At this stage, it is useful to estimate how much the artery can expand compared to latex for the same outer diameter, as this provides insight into the device's expected performance in a real arterial environment. To this end, a five-parameter Mooney–Rivlin hyperelastic model was employed to characterize the nonlinear mechanical behavior of the arterial wall. The corresponding range of c-parameters was adopted from previously reported studies [32,33], while possible arterial wall thickness values at this outer diameter as well as arterial tissue density and blood properties were taken from [34,35] and listed in Table 1. Under these conditions, the simulations were repeated to determine the average expansion along the outer artery wall on Fig. 2a, excluding the PDMS-covered region. Since the model incorporated a range of c-parameters and wall thickness values, the results yielded an expected range of arterial expansion. This range was then compared to the latex expansion, as illustrated in Fig. 3. While the latex can expand only up to 4.94 mm, the artery is capable of expanding to diameters ranging from 5.12 mm to 6.39 mm, corresponding to a dimensional increase of 0.35–1.62 mm and a percentage increase of 7–34 %, respectively. The PDMS expansion on the artery was also computed, yielding values between 0.29 mm (from 5.37 mm to 5.66 mm) and 0.98 mm (from 5.37 mm to 6.35 mm).

For magnetic simulations, magnets and sensors were added to the model as shown in Fig. 4a. Next, the evolution of the magnetic field inside the sensor module was simulated as a result of the pressure increase and the resulting PDMS expansion on latex, as shown in Fig. 2b.

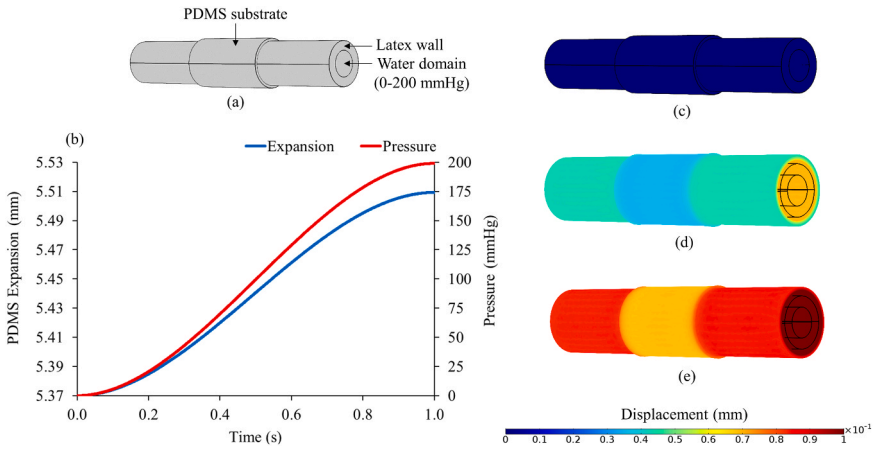

Fig. 2. (a) Simulation model showing latex and encircling PDMS substrate, (b) applied pressure profile and the resulting PDMS expansion on latex as a function of time, (c-e) the resulting latex and PDMS displacements for 0, 100 and 200 mmHg, respectively.

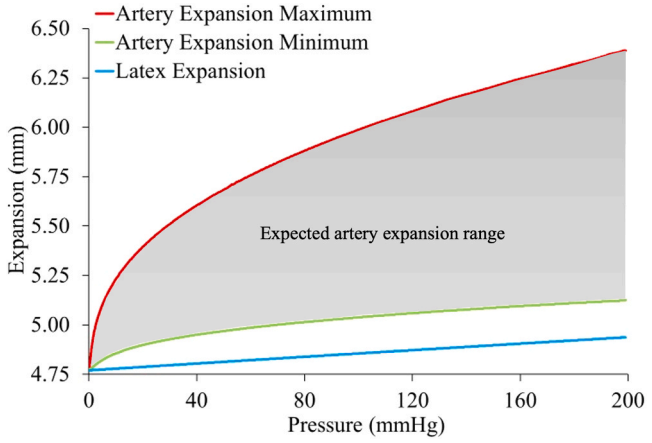

Fig. 3. Range of expected artery expansion in comparison to latex.

The circular collocations of the sensors and magnets was updated for every 20 mmHg increments, and the magnetic flux density acting on the sensor surfaces were analyzed. The rest of the geometric and material parameters used in the simulations are listed on Table 2. The magnetic flux density distributions on the bottom sensor surface for D0 and D1 at 0 mmHg and 200 mmHg are plotted on Fig. 4b-c. Due to the symmetry leading to the same magnetic flux density, simulation results for D2 are not shown.

The magnetic flux density distribution on top sensor surfaces were also simulated and an average flux density value were calculated for all the designs. Fig. 5 plots these values with respect to the PDMS expansion and also shows the representative magnetic field lines inside the sensor module. Since there are two sensors in D2, two flux densities on each sensor was added up as these sensors can be serially connected for a higher output voltage. It is clear that the flux lines are more effectively utilized on the sensors in D1 and D2 due to the number and placement of the magnets. The flux density variations exhibit a linear trend for all designs. The total reduction in the average magnetic fluxes were determined to be 0.192 mT, 0.767 mT, and 1.535 mT for D0-D2, respectively.

The detection sensitivity of each design can be defined as the slopes $\Delta B/\Delta Ø$ on Fig. 5, which establishes a figure of merit for comparison. In

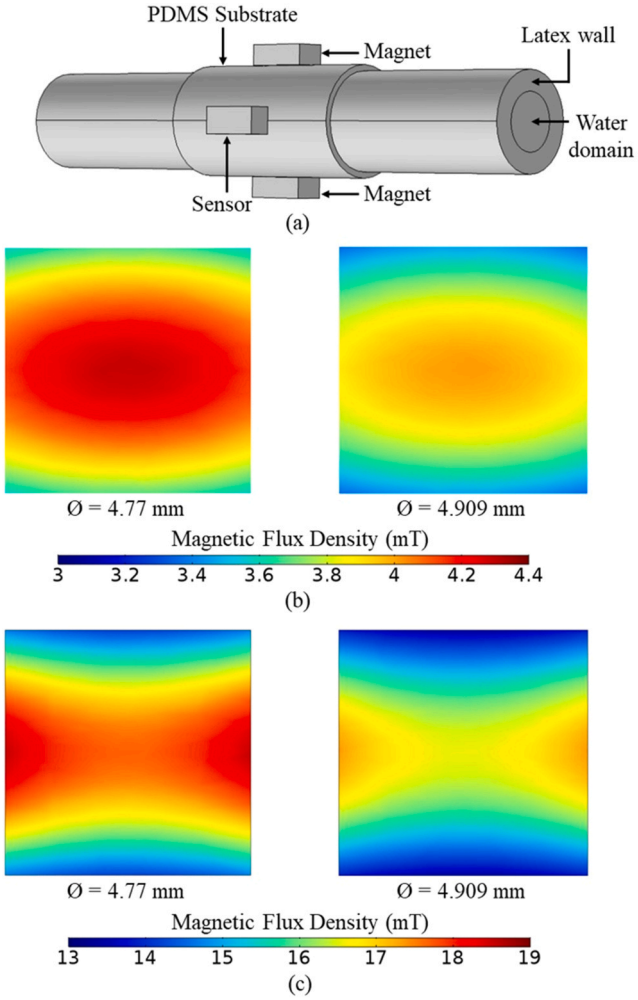

Fig. 4. (a) Magnetic simulation model for D1, and vertical magnetic flux density on bottom sensor surface for (b) D0 and (c) D1–2.

Table 2
Magnetic simulation parameters.

Parameter	Value	Parameter	Value
Sensor length	2.92 mm	Relative permeability (all domain)	1
Magnet length	3 mm	PDMS expansion	2.6 %
Sensor width	1.3 mm	Remanent flux density	1.39 T
Magnet width	1.5 mm	Magnet material	NdFeB
Sensor thickness	1.12 mm	Propagation media	Air
Magnet thickness	1 mm	PI thickness	0.13 mm

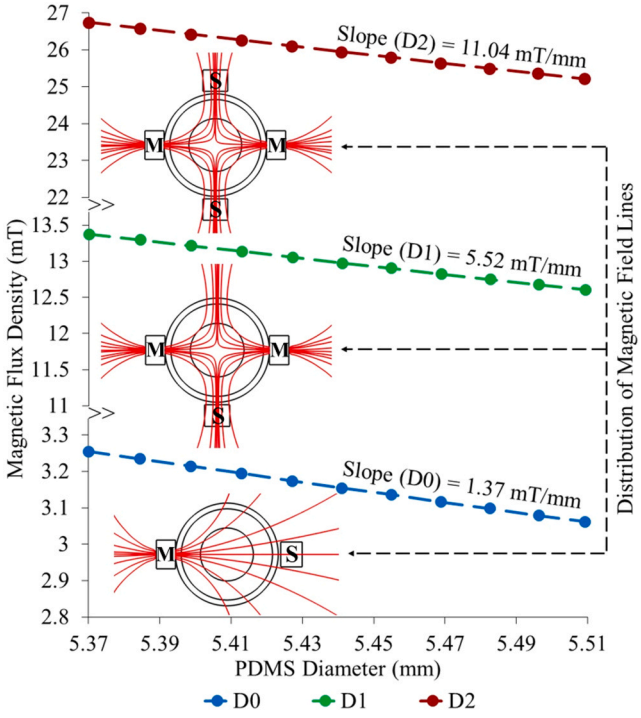

Fig. 5. Average magnetic flux density on sensors vs PDMS diameter for all designs.

this respect, D0-D2 yielded 1.37 mT/mm, 5.52 mT/mm and 11.04 mT/mm, respectively. This shows that D1 and D2 can provide 4- and 8-fold improvement compared to D0. This is more than the 2-fold increase one would expect due to using twice as many magnets, underlining the performance merit of our proposed designs. Using these sensitivity values together with the empirical relationship noted on the Hall sensor specifications, the sensor voltage v_{out} can be calculated according to the equation:

$$v_{out} = v_Q + B \times S_{(25°C)} \quad (1)$$

where v_Q is the quiescent voltage, B is the magnetic flux density acting on the sensor and $S_{(25°C)}$ is the magnetic sensitivity at 25°C. Using (1) together with the sensitivity of 200 mV/mT and the quiescent voltage of 600 mV as declared by the manufacturer, the estimated sensor voltages were calculated and plotted on Fig. 6 as a function of pressure. Accordingly, D0, D1 and D2 are expected to yield a total voltage difference of 38.4 mV, 153.4 mV and 306.8 mV across the investigated pressure range. These results dictate a final pressure sensitivity values of 0.192 mV/mmHg, 0.767 mV/mmHg and 1.534 mV/mmHg, respectively. These magnetic simulations and calculations were also repeated for the case in which the PDMS expands on an artery, as discussed previously. Because the expansion profiles shown in Fig. 3 are nonlinear, it is not possible to define a single sensitivity valid across the entire pressure range. Instead, an average sensitivity was calculated based on the voltage difference over the full range of pressures. Owing to the

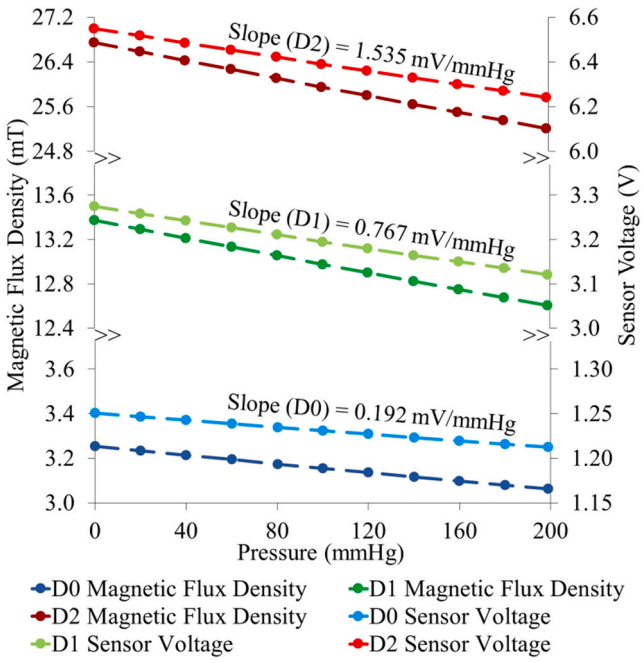

Fig. 6. Sensor voltage and magnetic flux density versus pressure for all designs.

larger relative displacements between components, the average sensitivity values in the PDMS expansion ranges were higher than those obtained with latex, measuring between 0.38 and 1.09 mV/mmHg, 1.54–4.37 mV/mmHg, and 3.07–8.74 mV/mmHg for D0, D1, and D2, respectively.

3. Fabrication

The sensor module was fabricated using a combination of material deposition, shadow masking, and 3D-printing technologies. Initially, a PLA structure was 3D-printed as a mold and fixed on a silicon wafer (Fig. 7a). PDMS silicone elastomer base and curing agent (Dow Chemical Company, Sylgard 184) were mixed at a weight ratio of 10:1 to achieve appropriate flexibility, and degassed in a vacuum chamber to remove all trapped air bubbles. Next, the PDMS was poured onto the mold and cured on the hot plate at 75 °C for 75 min (Fig. 7b), resulting in a final thickness of 300 μm. The length and width of the PDMS substrate were designed to be 10 mm and 28 mm, respectively, to ensure a firm artery grip. Following the substrate fabrication, the precise locations of the magnets and sensors were marked through metal deposition. In this respect, an acetate paper was laser cut and used as a shadow mask on the substrate (Fig. 7c). Next, a 100 nm-thick Cr layer was sputtered (Nanovak, NVTS-400) (Fig. 7d) and the shadow mask was removed (Fig. 7e). Finally, the substrate was cut and removed from the wafer (Fig. 7f).

A 0.13 mm thick PI substrate (Kapton tape 18-S, CS Hyde Company) was used to accommodate electrical connections for the Hall sensors. The tape was adhered on a silicon wafer (Fig. 8a) and a separate shadow mask with sensor pin and connection routing layout was fixed on it (Fig. 8b). Next, a 500 nm-thick layer of Cu was thermally evaporated (Nanovak, NVTS-400) on the tape (Fig. 8c). The mask was then removed and the Kapton tape was separated from the wafer (Fig. 8d-e). To establish the electrical contact between the sensor and the deposited Cu as well as to fix the sensor on the Kapton tape, a conductive epoxy kit (Epoxy Technology, EPO-TEK H20s) was mixed at a weight ratio of 1:1 and applied to the Cu surface (Fig. 8f). Subsequently, the sensor was carefully aligned and bonded to the contacts, and the epoxy was cured at 110 °C for 90 min to establish a strong bond (Fig. 8g). The Kapton tape with the Hall sensor was adhered to the PDMS substrate through a

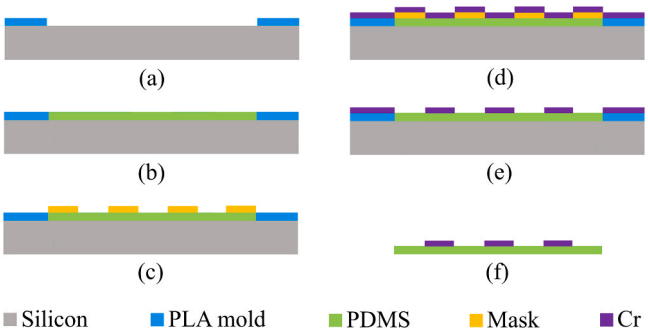

Fig. 7. Microfabrication flow of the substrate.

biocompatible epoxy (Epoxy Technology, EPO-TEK 302–3 M). For this step, the epoxy kits were mixed at a weight ratio of 10:4.5, applied on the PDMS, and cured at 100 °C for 30 min with the Kapton tape on top (Fig. 8h). Although not shown on Fig. 8, this same process step was also applied on the magnets to firmly mount them on the PDMS substrate. A final layer of the biocompatible epoxy was applied and cured over the top of the sensors and magnets to provide biocompatibility and to prevent the exposure of these components to body liquids (Fig. 8i). Electrical access to the sensors were made through copper wires bonded to the contact pads using the conductive epoxy. Photographs of the fabricated devices are shown in Fig. 9.

4. Experimental testing and discussion

In vitro experiments were performed to characterize the proposed sensor-magnet configurations. The schematic of the test setup is shown in Fig. 10. Initially, the fabricated sensor modules were wrapped around the latex pipe, which was preferred instead of the actual artery for the reasons discussed in the previous section, and fixed using a metal clip. A peristaltic pump (PT-500, Bimetron) was used to flow water through the latex pipe. In all experiments, the pump was set to produce pulses at a frequency of 2.5 Hz and push water into the system with a flow rate of 40 ml/min. It should be noted that the pulsatile nature of the pump does not allow to apply a constant water pressure, and rather yields oscillations in the pressure level. A flow valve was employed to set the average pressure level with such oscillations. In this setting, throttling or releasing the valve increases or decreases the pressure inside latex, respectively. A commercial pressure sensor (P51, SSI Technologies) was employed on the latex to measure the water pressure and correlate with the sensor module readings. The Hall sensor and the commercial pressure sensor were operated at 5 V through a power supply. Hall sensor data were acquired with an oscilloscope (MDO3024, Tektronix) at a sampling rate of 100 Hz.

Since the amount of latex expansion is critical on the final pressure sensitivity, the radial displacement of latex pipe was measured using a high resolution camera during pumping. To perform this measurement, the average water pressure was slowly increased from 0 to 200 mmHg, with pressure oscillations reaching ±45 mmHg at 200 mmHg. In the meantime, the diameter change in latex pipe was captured and processed with the camera at 60 fps and Kinovea software, respectively, while the pressure inside latex was acquired with the commercial pressure sensor. Fig. 11 shows that the diameter variation and the pressure readings closely match throughout the complete pressure range. The outer diameter of latex was measured to increase from 4.77 mm at 0 mmHg to 4.89 mm at 200 mmHg with a measurement error of ±0.04 mm. This corresponds to approximately 2.6 % expansion rate, as opposed to 3.56 % as predicted by the simulations above. This difference is mostly attributed to the Young's modulus of the commercial latex pipe not perfectly matching its theoretical value.

After determining the expansion rate of latex, all designs were tested in-vitro to compare their sensing performances. The testing pressure range was set to 0–200 mmHg, consistent with the range used in simulations. The water pressure was switched between these two pressure levels in a period of 40 s. Fig. 12 plots sensor voltages and applied pressure versus time for D0, D1 and D2. It is clearly seen from the graphs that there is a direct correlation between pressure and sensor voltage for all sensor modules. The variation in voltage values corresponding to 0 mmHg is attributed to the sensor noise that can reach 24 mV_{PP}, whereas the oscillations at 200 mmHg is due to the pulsatile pumping. These oscillations are at 2.5 Hz, which is well below the frequency detection limit of the Hall sensor.

All data points graphed on Fig. 12 are used in linear regression

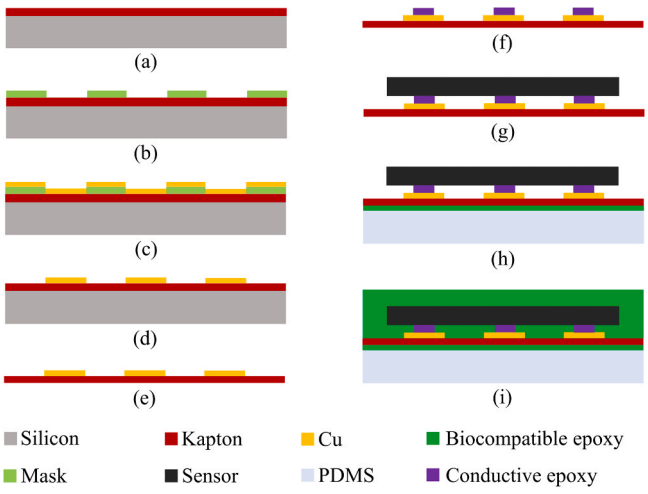

Fig. 8. Microfabrication flow of the sensor package on the substrate.

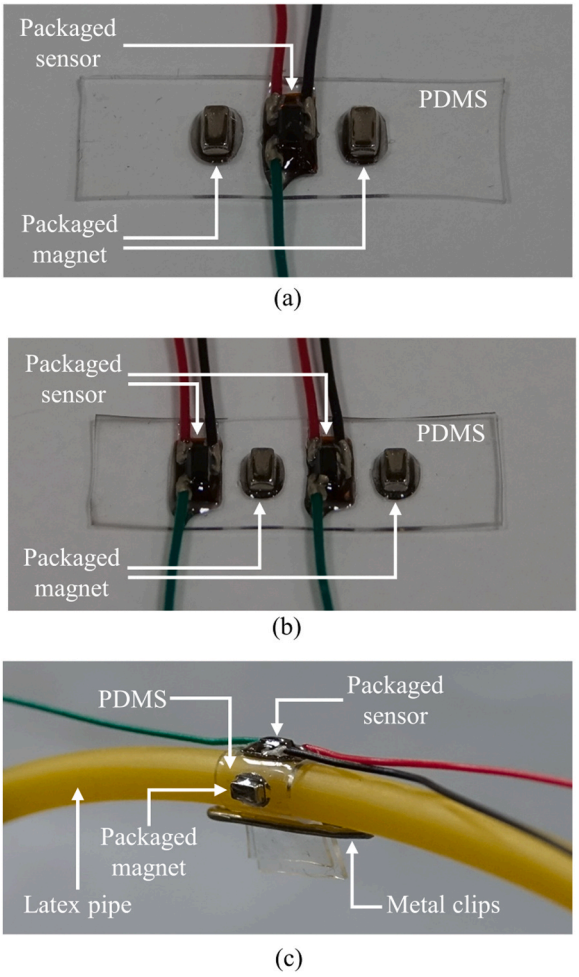

Fig. 9. Photographs of fabricated (a) D1, (b) D2 and (c) D1 fixed around latex pipe.

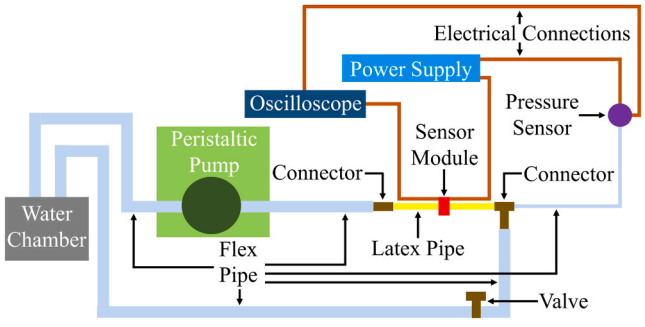

Fig. 10. The schematic of the test setup.

analysis to calculate the pressure-voltage correlation and sensitivity. Fig. 13 plots sensor voltages for D0, D1 and D2 versus applied pressure and their fitted data. The results show that D0, D1 and D2 yielded a total voltage difference of 22.4 mV, 52.2 mV and 84 mV in a pressure span of 0–200 mmHg. These results dictate final pressure sensitivity values of 0.112 mV/mmHg, 0.261 mV/mmHg and 0.42 mV/mmHg, respectively. This shows that D1 and D2 can provide 2.33- and 3.8-fold improvement compared to previously reported D0. Another improvement was also observed in linearity. A better correlation between pressure-voltage data was also demonstrated in the graphs for D1 ($R^2 = 0.9832$) and D2 ($R^2 = 0.9817$) compared to D0 ($R^2 = 0.9380$). Root mean square errors (RMSE) of D1 and D2 were calculated as 0.0032 V and 0.0056 V, which

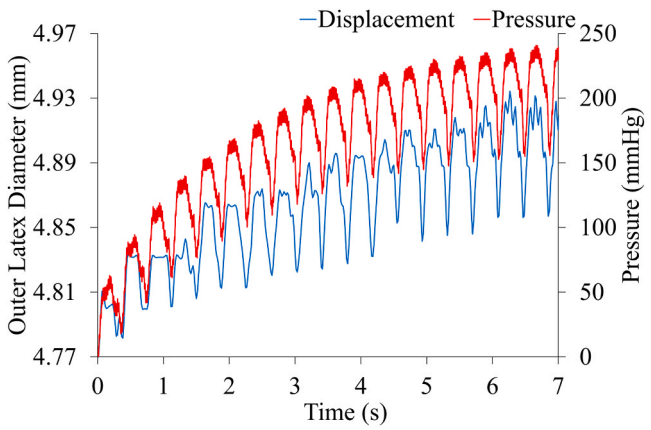

Fig. 11. Expansion of latex pipe and the water pressure inside as captured by a high speed camera and a commercial pressure sensor.

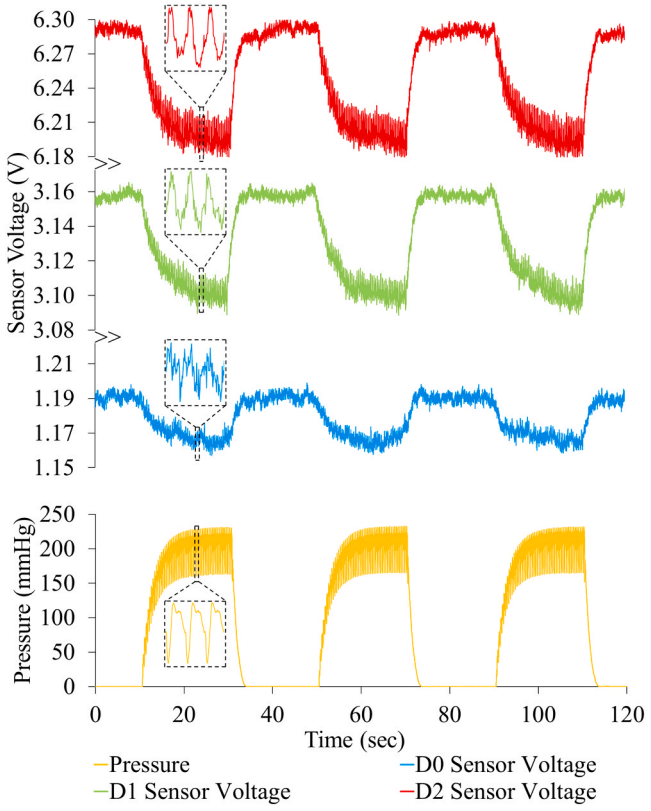

Fig. 12. Sensor voltage and applied pressure versus time for all designs in air.

indicate errors of 6.15 % and 6.66 %, respectively. D2 sensitivity should ideally be twice of D1 based on the simulation results. However, imperfect magnet and sensor placements during device assembly are believed to reduce $\Delta B/\Delta \emptyset$, and lead to this result. Under these circumstances, it was concluded that although D2 yielded a higher voltage difference, D1 showed better sensitivity per sensor. Therefore, the following tests were carried out using D1.

Long-term tests were carried out to investigate the reliability of D1. In this respect, voltage-pressure data was acquired for 5 days for a duration of 120 s each. As clearly seen on Fig. 14, the sensor module maintained the same voltage response and performance throughout the course of this test, and no detectable voltage variation was observed. The major factor in the long-term stability of D1 stems from the ability of PDMS and latex to stretch together elastically without undergoing

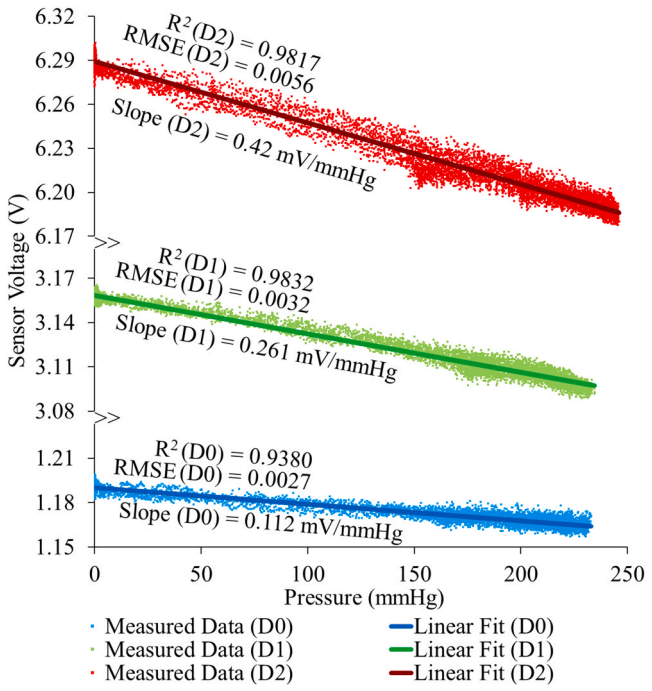

Fig. 13. Sensor voltage for all designs versus applied pressure and their fitted data.

permanent mechanical deformations under pressure, as well as good adhesion of the sensor and magnets to the PDMS.

Durability and sealing reliability of D1 was also investigated in Phosphate-Buffered Saline (PBS) solution that mimics the body environment. In this respect, the sensor module was fixed around the latex and immersed in PBS (pH = 7.4), and its in vitro-liquid sensing performance was monitored. Fig. 15 graphs the sensor voltage and applied pressure versus time for D1. A very similar correlation as that in Fig. 12 in air was obtained. The regression analysis plotted on Fig. 16 shows a very high linearity (R2 = 0.9823), low error (RMSE=0.0033) and a sensitivity of 0.263 mV/mmHg, which is almost the same as the in-air performance. This also demonstrates that although there was a slight decrease in the high and low voltage levels of D1, the sensitivity and linearity were maintained. Finally, long-term tests in PBS were performed with D1 and the results are plotted on Fig. 17. It is seen from the graph that the sensor voltage followed the same trend for 5 days. In addition, no visible change on the sensor module was observed, indicating the physical sturdiness inside PBS. This demonstrates the effectiveness of the biocompatible packaging and confirms the stability of the sensor module when used within the body.

Theoretical and experimental results demonstrate that the designs D1 and D2, developed in this work, offer a notable improvement in sensitivity and linearity compared to the previously reported state-of-the-art design, D0. Experimental sensitivity values were found to be lower compared to the simulation results. This is attributed to (i) the magnets having a magnetization below their maximum potential (ii) voltage drops across the connection pads and wires and (iii) imperfections in the placement of magnets and sensors. Long term tests in air demonstrated the reliability of the sensor module, while the same tests in PBS proved its durability in a biological environment. The reported sensitivity values were obtained using a commercial latex pipe, which exhibited a radial expansion limited to approximately 2.6 % of its diameter under the applied pressure range. While suitable as a simple experimental model, this material response substantially underestimates the mechanical behavior of arterial tissue. Our simulation results demonstrate that arterial walls can expand by 7–34 % under the same pressure range, depending on their mechanical properties and wall

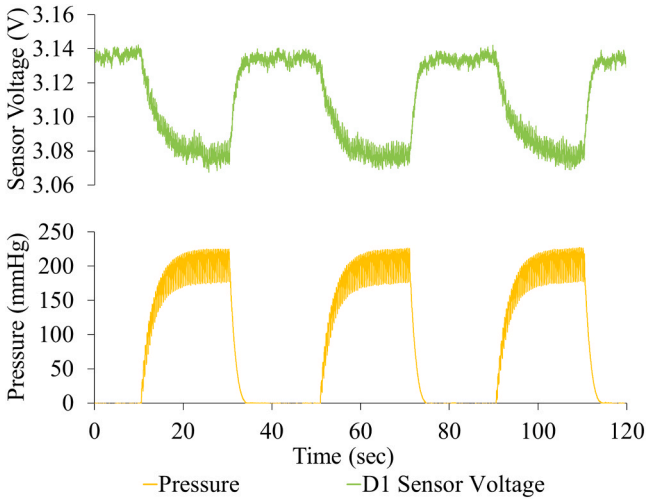

Fig. 15. Sensor voltage and applied pressure versus time for D1 immersed in PBS.

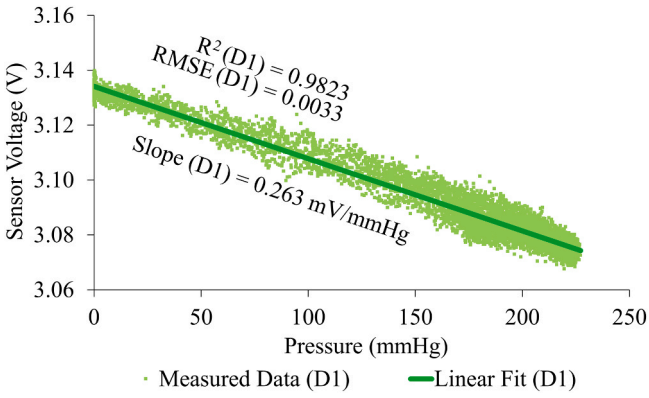

Fig. 16. Sensor voltage for D1 immersed in PBS versus applied pressure and fitted data.

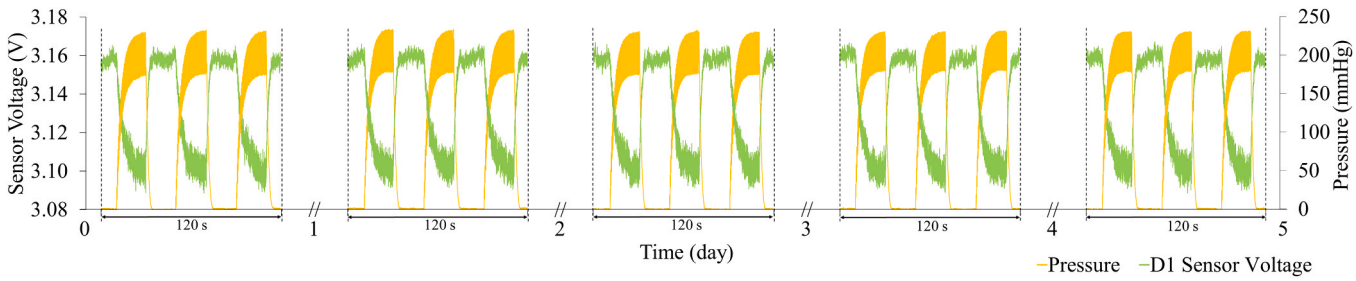

Fig. 14. Sensor voltage of D1 and applied pressure versus time for 5 days.

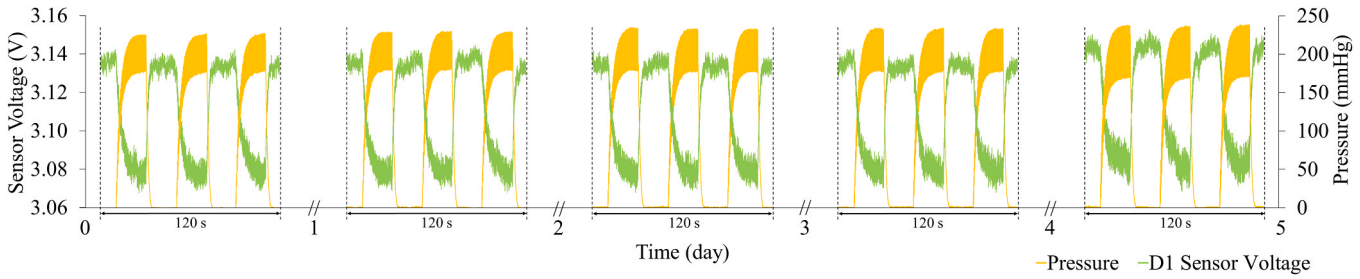

Fig. 17. Sensor voltage for D1 immersed in PBS and applied pressure versus time for 5 days.

thickness. Assuming an average expansion of 20 % and considering the highly linear response of the sensor module, the average sensitivity is projected to reach up to 2 mV/mmHg for D1 and 3.2 mV/mmHg for D2. It is important to note that the complex biological structure of the arterial wall may introduce additional nonlinearities that were not accounted for in the simulations described above. Moreover, larger relative displacements of the sensor module on the artery, beyond the range shown in Fig. 5, may also introduce nonlinearities in the flux density–diameter relationship. These factors may lead to deviations from the projected sensitivity values. To achieve accurate pressure readings, the sensor module can be calibrated once during implantation using a surgical-grade blood pressure monitor. Systolic, diastolic, and intermediate pressure values can then be matched to the corresponding output voltages, after which the sensor operates independently to provide reliable measurements. This sensitivity value can be further enhanced by using higher-grade stronger magnets and higher number of magnets on the sensor module. This may also pose challenges in the manufacturing of the sensor module due to higher repulsive forces.

5. Conclusion

Magnetic sensing modules composed of multiple Hall sensors and permanent magnets for in-vivo blood pressure measurement were presented. The components were mounted on a flexible substrate, and arranged in a configuration optimized to produce maximum voltage in response to arterial distension. The components were packaged using biocompatible materials and tested on a latex pipe. Experimental results revealed up to 3.8-fold improvement in pressure sensitivity and better linearity compared to the basic magnet-sensor pair. Long-term experiments in PBS solution showed virtually no change in the sensitivity. The maximum average sensitivity of the modules is projected to reach 3.2 mV/mmHg when implanted on an artery. These results demonstrate the suitability of the sensor modules presented here for blood pressure monitoring inside the body after anastomosis procedures. Further studies will focus on integrating the modules with a biotelemetry system to enable wireless pressure tracking from outside the body.

CRediT authorship contribution statement

Mustafa İlker Beyaz: Writing – review & editing, Writing – original draft, Supervision, Project administration, Methodology, Investigation, Funding acquisition, Formal analysis, Conceptualization. **Tuğba Selcen Navruz:** Writing – review & editing, Supervision. **Menduh Furkan Aslan:** Writing – original draft, Validation, Software, Methodology, Formal analysis, Data curation.

Declaration of generative ai and Ai-assisted technologies in the writing process

During the preparation of this work, the authors used ChatGPT to improve the clarity and fluency of the English language. After using this tool, the authors reviewed and edited the content as needed, and take full responsibility for the publication's content.

Declaration of Competing Interest

The authors declare no conflict of interest.

Acknowledgments

This work was supported by The Scientific and Technological Research Council of Türkiye (TUBITAK) under grant number 121E369, and carried out at Antalya Bilim University Micro/Nano Devices Laboratory. The authors would like to thank Asst. Prof. Dr. Seda DEMİREL TOPEL for providing PBS solution.

Data availability

Data will be made available on request.

References

[1] Global Observatory on Donation and Transplantation (GODT), "Organs Ttransplanted Annually 2023," Available: https://www.transplant-observatory.org/, Accessed on: July 2, 2024.
[2] G.T. Um, et al., Implantable Cook-Swartz Doppler probe versus Synovis Flow Coupler for the post-operative monitoring of free flap breast reconstruction, J. Plast. Reconstr. Aesthetic Surg. 67 (7) (Jul. 2014) 960–966, https://doi.org/10.1016/j.bjps.2014.03.034.
[3] W.M. Swartz, N.F. Jones, L. Cherup, A. Klein, Direct monitoring of microvascular anastomoses with the 20-MHz ultrasonic Doppler probe: an experimental and clinical study, Plast. Reconstr. Surg. 81 (2) (Feb. 1988) 149–158.
[4] G. Ogedegbe, T. Pickering, Principles and Techniques of Blood Pressure Measurement, Cardiol. Clin. 28 (4) (Nov. 2010) 571–586, https://doi.org/10.1016/j.ccl.2010.07.006.
[5] F. Springer, R.W. Günther, T. Schmitz-Rode, Aneurysm Sac Pressure Measurement with Minimally Invasive Implantable Pressure Sensors: An Alternative to Current Surveillance Regimes after EVAR? Cardiovasc. Interv. Radiol. 31 (3) (Dec. 2007) 460–467, https://doi.org/10.1007/s00270-007-9245-9.
[6] L. Wang, et al., The PolyCraft Polymer–Metal Hybrid Smart Stent System: The Future of Cardiovascular Blood Pressure Management, Adv. Funct. Mater. 34 (46) (Aug. 2024), https://doi.org/10.1002/adfm.202408022.
[7] K. Kwon, et al., A battery-less wireless implant for the continuous monitoring of vascular pressure, flow rate and temperature, Nat. Biomed. Eng. 7 (10) (May 2023) 1215–1228, https://doi.org/10.1038/s41551-023-01022-4.
[8] A. Bulbul, H. Kim, Pressure Sensor Embedded Inductive Coil Toward a Wireless Pressure Sensing Stent, J. Micro Syst. 30 (2) (Apr. 2021) 224–233, https://doi.org/10.1109/jmems.2020.3049085.
[9] P. Bingger, M. Zens, P. Woias, Highly flexible capacitive strain gauge for continuous long-term blood pressure monitoring, Biomed. Micro 14 (3) (Feb. 2012) 573–581, https://doi.org/10.1007/s10544-012-9636-9.
[10] C.M. Boutry, et al., Biodegradable and flexible arterial-pulse sensor for the wireless monitoring of blood flow, Nat. Biomed. Eng. 3 (1) (Jan. 2019) 47–57, https://doi.org/10.1038/s41551-018-0336-5.
[11] M. Theodor, et al., Implantable accelerometer system for the determination of blood pressure using reflected wave transit time, Sens. Actuators A Phys. 206 (Dec. 2013) 151–158, https://doi.org/10.1016/j.sna.2013.12.006.
[12] K.-H. Shin, C.-Y. Moon, T.-H. Lee, C.-H. Lim, Y.-J. Kim, Implantable flexible wireless pressure sensor module, Sens Vienna Austria (2004) 844–847.
[13] J. Ruhhammer, et al., Arterial strain measurement by implantable capacitive sensor without vessel constriction, 2012 Annu. Int. Conf. IEEE Eng. Med. Biol. Soc. San. Diego CA USA (2012) 535–538.
[14] P. Cong, W.H. Ko, D.J. Young, Wireless Batteryless Implantable Blood Pressure Monitoring Microsystem for Small Laboratory Animals, IEEE Sens. J. 10 (2) (Feb. 2010) 243–254, https://doi.org/10.1109/jsen.2009.2030982.
[15] S.R.A. Ruth, et al., Post-surgical wireless monitoring of arterial health progression, iScience 24 (9) (Sep. 2021) 103079, https://doi.org/10.1016/j.isci.2021.103079.

[16] J.A. Potkay, K. Brooks, "An Arterial Cuff Energy Scavenger For Implanted Microsystems, 2008 2nd Int. Conf. Bioinforma. Biomed. Eng. Shanghai China (2008) 1580–1583.
[17] X. Cheng, et al., Implantable and self-powered blood pressure monitoring based on a piezoelectric thinfilm: Simulated, in vitro and in vivo studies, Nano Energy 22 (Apr. 2016) 453–460, https://doi.org/10.1016/j.nanoen.2016.02.037.
[18] C. Wang, et al., Tissue-Adhesive Piezoelectric Soft Sensor for In Vivo Blood Pressure Monitoring During Surgical Operation, Adv. Funct. Mater. 33 (38) (May 2023), https://doi.org/10.1002/adfm.202303696.
[19] C. Tang, et al., Unconstrained Piezoelectric Vascular Electronics for Wireless Monitoring of Hemodynamics and Cardiovascular Health, Small 20 (3) (Sep. 2023), https://doi.org/10.1002/smll.202304752.
[20] M. Besirli, et al., An Implantable Wireless System for Remote Hemodynamic Monitoring of Heart Failure Patients, IEEE Trans. Biomed. Circuits Syst. 17 (4) (May 2023) 688–700, https://doi.org/10.1109/tbcas.2023.3273711.
[21] N. Inoue, Y. Koya, N. Miki, H. Onoe, Graphene-Based Wireless Tube-Shaped Pressure Sensor for In Vivo Blood Pressure Monitoring, Micromachines 10 (2) (Feb. 2019) 139, https://doi.org/10.3390/mi10020139.
[22] Y. Hacohen, S.J. Majerus, A Flexible Double Helix Inductive Antenna for RFID Vascular Flow Sensing, IEEE Sens. J. 23 (17) (Jul. 2023) 19044–19051, https://doi.org/10.1109/jsen.2023.3291172.
[23] M. Theodor, et al., Subcutaneous blood pressure monitoring with an implantable optical sensor, Biomed. Micro 15 (5) (May 2013) 811–820, https://doi.org/10.1007/s10544-013-9768-6.
[24] J. Fiala, et al., An implantable optical blood pressure sensor based on pulse transit time, Biomed. Micro 15 (1) (Sep. 2012) 73–81, https://doi.org/10.1007/s10544-012-9689-9.
[25] M. Theodor, et al., Implantable Impedance Plethysmography, Sensors 14 (8) (Aug. 2014) 14858–14872, https://doi.org/10.3390/s140814858.
[26] K. Zhu, A. Kiourti, A Review of Magnetic Field Emissions From the Human Body: Sources, Sensors, and Uses, IEEE Open J. Antennas Propag. 3 (2022) 732–744, https://doi.org/10.1109/OJAP.2022.3186643.
[27] J. Ruhhammer, et al., "Magnetic sensor for monitoring of arterial strain, TRANSDUCERS Eur. XXVII 17th Int. Conf. SolidState Sens. Actuators Microsyst. (TRANSDUCERS Eur. XXVII) Barc. Spain 2013 (2013) 1667–1670.
[28] M.F. Aslan, O. Kerbouche, T.S. Navruz, M.İ. Beyaz, "A Magnetic Sensor for Artery Pressure Monitoring, 2023 11th Int. Jpn. Afr. Conf. Electron. Commun. Comput. (JACECC) Alex. Egypt (2023) 277–280.
[29] C. Wang, et al., Monitoring of the central blood pressure waveform via a conformal ultrasonic device, Nat. Biomed. Eng. 2 (9) (Sep. 2018) 687–695, https://doi.org/10.1038/s41551-018-0287-x.
[30] X.M. Zhang, J.F. Greenleaf, An anisotropic model for frequency analysis of arterial walls with the wave propagation approach, Appl. Acoust. 68 (9) (Jun. 2006) 953–969, https://doi.org/10.1016/j.apacoust.2006.04.014.
[31] X. Zhang, J.F. Greenleaf, Generation of a torsion wave and measuring its propagation velocity in the circumferential direction of arterial wall, Ultrasonics 44 (Dec. 2006) 165–168, https://doi.org/10.1016/j.ultras.2006.06.054.
[32] M. Imani, A.M. Goudarzi, D.D. Ganji, A.L. Aghili, The comprehensive finite element model for stenting: the influence of stent design on the outcome after coronary stent placement, J. Theor. Appl. Mech. 51 (3) (2025) 639–648.
[33] D. Wang, F. Serracino-Inglott, J. Feng, Numerical simulations of patient-specific models with multiple plaques in human peripheral artery: a fluid-structure interaction analysis, Biomech. Model. Mechanobiol. 20 (1) (Sep. 2020) 255–265, https://doi.org/10.1007/s10237-020-01381-w.
[34] D.B. Camasão, D. Mantovani, The Mechanical Characterization of Blood Vessels and Their Substitutes in the Continuous Quest for physiological-relevant performances. a Critical Review, Mater. Today Bio 10 (10) (Mar. 2021) 100106, https://doi.org/10.1016/j.mtbio.2021.100106.
[35] D. Lopes, H. Puga, J.C. Teixeira, S.F. Teixeira, Influence of arterial mechanical properties on carotid blood flow: Comparison of CFD and FSI studies, Int. J. Mech. Sci. 160 (Sep. 2019) 209–218, https://doi.org/10.1016/j.ijmecsci.2019.06.029.

Menduh Furkan Aslan received his B.S. degree in Electrical and Electronics Engineering from Dokuz Eylul University in 2016 and M.S. degree in Electrical and Electronics Engineering from Süleyman Demirel University in 2018. He is a Ph.D. candidate at Gazi University since 2020. He joined Antalya Bilim University as a research assistant in 2017. His research focuses on the development of micro- and nano-scale flexible, implantable and wearable sensors for biomedical applications.

Tuğba Selcen Navruz received her B.S., M.S., and Ph.D degrees in Electrical and Electronics Engineering from Gazi University in 1997, 2002, and 2008, respectively. She joined Gazi University as a faculty member in 2009. She has been at University of California, Los Angeles, EE Faculty, Integrated NanoMaterials Core Lab as a visiting scholar in 2011. Her research studies are focused on photovoltaic solar cells, and semiconductor device modeling. Her recent studies include sensor technologies and sensor fusion for robot mapping, and localization applications.

Mustafa Ilker Beyaz received his B.S. degree in Electrical and Electronics Engineering from the Middle East Technical University in 2005, and his M.S and Ph.D degrees in Electrical Engineering from the University of Maryland College Park in 2008 and 2011, respectively. He joined Antalya Bilim University as a faculty member in 2011, where he led research activities in the development of MEMS sensors, actuators, and energy harvesters for biomedical applications. Dr. Beyaz later joined the Institute of Microstructure Technology at Karlsruhe Institute of Technology as a research scientist in 2023. His research interests include the development of micro- and nano-scale systems for medical technologies, as well as the application of MEMS in the field of Nuclear Magnetic Resonance.